

Behaviour of pf shell under RMF+BCS Description

G. Saxena^a, M. Kaushik^b

^a*Department of Physics, Govt. Women Engineering College, Ajmer-305002, India*

^b*Department of Physics, Shankara Institute of Technology, Kukas, Jaipur-302028, India*

Abstract

We have employed RMF+BCS (relativistic mean-field plus BCS) approach to study behaviour of pf shell with the help of ground state properties of even-even nuclei. Our present investigations include separation energies, deformations, single particle energies, wavefunction, potential as well etc density distribution. As per recent experiments showing neutron magicity at $N = 32$ for Ca isotopes, our results with mass dependent pairing indicate a shell closure at $N = 32$ in Ca isotopes and a more strong shell closure at $N = 34$ in proton deficient ^{48}Si because of reorganization of neutron pf shell. In a similar manner, proton pf shell structure is more likely to produce shell closure at $Z = 34$ with a doubly magic character for $^{84,116}\text{Se}$. We have also included $N = 40$ isotones and $Z = 40$ isotopes for our study and predicted ^{60}Ca and ^{68}Ni as doubly magic nuclei out of which ^{60}Ca is found near drip-line of Ca and a potential candidate for future studies in the chain of Ca isotopes next to doubly magic ^{52}Ca .

Keywords: Neutron and proton magic nuclei; Relativistic mean-field plus BCS approach; pf shell nuclei; Doubly Magic Nuclei, Shell Closure.

1. Introduction

Evolution of shell structure is being a momentous topic in the world of theoretical and experimental nuclear physics since last two decades. There are several regions of periodic chart which have been established showing new magicity or showing disappearance of traditional magicity through different theoretical approaches and confirmed from many experiments. As an example, appearance of the new magic number $N = 16$ [1, 2, 3] has been corroborated and neutron drip-line nucleus ^{24}O with $N = 16$, is now considered as a doubly-closed-shell nucleus [2, 3, 4]. On the other hand disappearance of

the conventional magic numbers $N = 8, 20$ and 28 have been demonstrated through many communications [5] - [11].

In recent past, experimental studies strongly indicate $N = 32$ as a new magic number in Ca isotopes due to the high energy of the first 2^+ state in this nucleus [12]. In addition, high precision mass measurements were performed for the neutron rich Ca isotopes ^{53}Ca and ^{54}Ca by employing the mass spectrometer of ISOLTRAP at CERN and confirmed the magicity of the nucleus ^{52}Ca [13]. Furthermore, first experimental spectroscopic study on lowlying states was performed also with proton knockout reactions at RIKEN indicating the magic nature of the nucleus ^{54}Ca [14]. More recently, in 2015, $N = 32$ shell closure is confirmed for exotic isotopes $^{52,53}\text{K}$ in Ref. [15].

These recent evidences for emerging sub-shell gaps at neutron number $N = 32$ and $N = 34$ have accumulated high interest for the description of pf-shell nuclei [16, 17, 18]. The next benchmark in this region of pf shell after $N = 32$ and $N = 34$ is $N = 40$ [19], which is important in determining nuclear structure and likely also the location of the neutron drip-line in the Ca isotopic chain [20].

The theoretical studies of such nuclei can be in general grouped into three different approaches. These are (i) the ab initio methods, (ii) the macroscopic models with shell corrections and (iii) the self-consistent mean-field and shell model theories. As far as mean field models are concern there are mainly three nuclear mean-field models which are widely used in current calculations and are based on (i) the Skyrme zero range interaction initially employed by Vautherin and Veneroni [21], and Vautherin and Brink [22], (ii) the Gogny force [23] with finite range, and (iii) the relativistic mean-field model formulated by Walecka [24], and Boguta and Bodmer [25]. During the last several years, theoretical studies of neutron and proton rich nuclei away from the valley of β -stability have been mostly accomplished under the framework of mean-field theories [26, 27, 28, 29], and also employing their relativistic counterparts [24, 25, 30, 31, 32, 33, 34, 35, 36, 37, 38, 39, 40, 41, 42]. Recently, the interest in tensor interaction for nuclear structure has also been revived by the study of the evolution of nuclear properties far from the stability line [17, 43, 44]. However, in the context of the effective theories that describe medium-heavy nuclei, the role of the tensor force is still debated [45].

In this paper, we will target pf shell nuclei with $N(Z) = 32$ and 34 along with the nuclei with $N(Z) = 40$ to study shell evolution for complete chain

of isotones(isotopes) upto drip-lines (covering mass region from $A = 48$ to $A = 122$). When nuclei move away from stability line toward their drip-lines then corresponding Fermi surface moves closer to zero energy at the continuum threshold and therefore significant number of the available single-particle states form part of the continuum. Since pairing correlations are very important for drip-line nuclei therefore to include them together with a realistic mean-field, the HF+BCS and RMF+BCS calculations has turned out to be very useful and successful tool as has been demonstrated recently [46, 47]. The principal advantage of the RMF approach is that it provides the spin-orbit interaction in the entire mass region in a natural way. Since the single particle properties near the threshold are prone to large changes as compared to the case of deeply bound levels in the nuclear potential therefore RMF approach has proved to be very crucial for the study of unstable nuclei upto the drip-lines. The results provided by RMF+BCS scheme [47, 48] are indeed in close agreement with the experimental data and other similar mean-field calculations [20]. In our investigations of pf shell nuclei, we use RMF+BCS approach to calculate ground state properties viz. single particle energy, deformation, separation energy as well as pairing energy etc. The results are compared with recent experimental results and various popular force parameters viz. TMA [49], NLSH [50], NL3 [51], PK1 [52] and NL3* [53] to bear witness of our results and outcomes. These above sets of parameters are for non-linear interaction and have been commonly used for variety of mass calculations for whole periodic region [34, 35, 40, 48, 54] with a very good agreement with available experimental data for whole mass table. Meanwhile, the new parameter sets belong to density dependent coupling are DD-ME1 [55], DD-ME2 [56], DD-ME δ [57] which have also provided a more realistic description of neutron matter and finite nuclei. However, due to few limitations of these density dependent coupling in describing several transitional medium-heavy nuclei [58] and to make a simplified and general treatment, we here prefer non-linear coupling to describe our results of pf shell nuclei which may posses transitional character [10, 59, 60]. The non linear interaction in RMF theory has proven to be very much effective, consistent and reliable [40, 41, 42, 46, 47, 48] and has recently successfully applied to study deformed nuclei at proton drip line [61], in the study of neutron star [62], in describing properties of superheavy nuclei [63] and determining hadron-quark phase transition line in the QCD phase diagram [64]. Therefore, we strongly believe that conclusions drawn here using RMF+BCS calculations with non linear effective interaction will not be affected very much by other

interactions or approaches.

2. Relativistic Mean-Field Model

The calculations have been carried out using the following model Lagrangian density with nonlinear terms both for the σ and ω mesons as described in detail in Refs. [33, 40, 48].

$$\begin{aligned}
\mathcal{L} = & \bar{\psi}[\not{\partial} - M]\psi \\
& + \frac{1}{2} \partial_\mu \sigma \partial^\mu \sigma - \frac{1}{2} m_\sigma^2 \sigma^2 - \frac{1}{3} g_2 \sigma^3 - \frac{1}{4} g_3 \sigma^4 - g_\sigma \bar{\psi} \sigma \psi \\
& - \frac{1}{4} H_{\mu\nu} H^{\mu\nu} + \frac{1}{2} m_\omega^2 \omega_\mu \omega^\mu + \frac{1}{4} c_3 (\omega_\mu \omega^\mu)^2 - g_\omega \bar{\psi} \gamma^\mu \psi \omega_\mu \\
& - \frac{1}{4} G_{\mu\nu}^a G^{a\mu\nu} + \frac{1}{2} m_\rho^2 \rho_\mu^a \rho^{a\mu} - g_\rho \bar{\psi} \gamma_\mu \tau^a \psi \rho^{\mu a} \\
& - \frac{1}{4} F_{\mu\nu} F^{\mu\nu} - e \bar{\psi} \gamma_\mu \frac{(1 - \tau_3)}{2} A^\mu \psi , \tag{1}
\end{aligned}$$

In the above Lagrangian the field tensors H , G and F for the vector fields are defined by

$$\begin{aligned}
H_{\mu\nu} &= \partial_\mu \omega_\nu - \partial_\nu \omega_\mu \\
G_{\mu\nu}^a &= \partial_\mu \rho_\nu^a - \partial_\nu \rho_\mu^a - 2g_\rho \epsilon^{abc} \rho_\mu^b \rho_\nu^c \\
F_{\mu\nu} &= \partial_\mu A_\nu - \partial_\nu A_\mu
\end{aligned}$$

and other symbols have their usual meaning.

Now, one can apply the BCS approximation to the state-independent pairing force but high density of single-particle states in the particle continuum immediately results in an unrealistic increase of BCS pairing correlations [65]. To avoid such an increase, one may artificially readjust the pairing strength constant but then the spatial asymptotic properties of the solutions become incorrect and consequently due to a nonzero occupation probability of quasibound states, there appears an unphysical gas of neutrons surrounding the nucleus [66]. These deficiencies can be healed by applying state-dependent-pairing-gap version, where the pairing gap is calculated for every single-particle state. But it is found that even with state dependent BCS calculations a surplus density above asymptotic limit appears at large distances

results incorrect behavior of the density [66]. Therefore, one may think that excluding the scattering states from the pairing phase space could be a decisive solution to the problem. Indeed, such scheme has been introduced by Sandulescu et al. [67] in which the effect of the resonant continuum on pairing correlations is introduced through the scattering wave functions located in the region of the resonant states. These states are found by solving the relativistic mean field equations with scattering-type boundary conditions for continuum spectrum and this scheme rBCS is found very effective for the description of drip line nuclei [67].

In this paper, for the chain of Ca and Ni isotopes, we have found resonant states $1g_{9/2}$ and $1g_{7/2}$ respectively but these states start to play an important role with their resonant part for $N > 40$ and $N > 50$ respectively. With this in view, these contributions of resonant states are less significant in terms of discussion of pf shells considered in this paper where we are concern upto $N = 40$ only. Moreover, we are mainly dealing with doubly magic nuclei in this paper and for doubly magic nuclei results of RMF+BCS and RMF+rBCS (including resonant part by Sandulescu et al. [67]) are found exactly same because for doubly magic nucleus pairing energy vanishes and resonant state does not contribute in the pairing energy. Therefore, in the context of this paper where we target only for pf shell nuclei (N or $Z \leq 40$), it is reasonable to perform state dependent BCS calculations [68, 69] based on single-particle spectrum in which continuum is replaced by a set of positive energy states generated by enclosing the nucleus in a spherical box. We have chosen box radius $R = 30$ fm which is same as has been taken in Ref [40, 41, 46, 47] and results are not much affected by changing the box radius around $R = 30$ fm at least for the considered doubly magic nuclei in pf shell.

Thus the gap equations have the standard form for all the single particle states, i.e.

$$\Delta_{j_1} = -\frac{1}{2} \frac{1}{\sqrt{2j_1 + 1}} \sum_{j_2} \frac{\langle (j_1^2) 0^+ | V | (j_2^2) 0^+ \rangle}{\sqrt{(\varepsilon_{j_2} - \lambda)^2 + \Delta_{j_2}^2}} \sqrt{2j_2 + 1} \Delta_{j_2} \quad (2)$$

where ε_{j_2} are the single particle energies, and λ is the Fermi energy, whereas the particle number condition is given by $\sum_j (2j + 1)v_j^2 = N$. In the calculations we use for the pairing interaction a delta force, i.e., $V = -V_0\delta(r)$. Initially, we use the same value of V_0 for our present study ($V_0 = 350$ MeV fm³) which was determined in Ref. [41] by obtaining a best fit to the binding energy of Ni isotopes. Since, we are covering region from $A = 48$ to

$A = 122$ therefore we will examine our results using mass dependent ($1/A$ -dependency) pairing strength which may be an effective way to handle large mass region. Apart from its simplicity, the applicability and justification of using such a δ -function form of interaction has been discussed in Ref. [70], whereby it has been shown in the context of HFB calculations that the use of a delta force in a finite space simulates the effect of finite range interaction in a phenomenological manner (see also [71] for more details). The pairing matrix element for the δ -function force is given by

$$\langle (j_1^2) 0^+ | V | (j_2^2) 0^+ \rangle = -\frac{V_0}{8\pi} \sqrt{(2j_1 + 1)(2j_2 + 1)} I_R \quad (3)$$

Here V_0 is the pairing strength which is taken as 350 MeV fm^3 for initial calculations and then it is used with mass dependency for further calculations as mentioned above. Mass dependent pairing strength used here is given by

$$V_0 = \frac{25,500}{A} \text{MeV fm}^3 \quad (4)$$

In equation (3), I_R is the radial integral having the form

$$I_R = \int dr \frac{1}{r^2} (G_{j_1}^* G_{j_2} + F_{j_1}^* F_{j_2})^2 \quad (5)$$

Here G_α and F_α denote the radial wave functions for the upper and lower components, respectively, of the nucleon wave function expressed as

$$\psi_\alpha = \frac{1}{r} \begin{pmatrix} i G_\alpha \mathcal{Y}_{j_\alpha l_\alpha m_\alpha} \\ F_\alpha \sigma \cdot \hat{r} \mathcal{Y}_{j_\alpha l_\alpha m_\alpha} \end{pmatrix}, \quad (6)$$

and satisfy the normalization condition

$$\int dr \{|G_\alpha|^2 + |F_\alpha|^2\} = 1 \quad (7)$$

In Eq. (6) the symbol \mathcal{Y}_{jlm} has been used for the standard spinor spherical harmonics with the phase i^l . The coupled field equations obtained from the Lagrangian density in (1) are finally reduced to a set of simple radial equations which are solved self consistently along with the equations for the state dependent pairing gap Δ_j and the total particle number N for a given nucleus.

The relativistic mean field description has been extended for the deformed nuclei of axially symmetric shapes by Gambhir, Ring and their collaborators [32] using an expansion method. The scalar, vector, isovector and charge densities, as in the spherical case, are expressed in terms of the spinor π_i , its conjugate π_i^+ , operator τ_3 etc. These densities serve as sources for the fields $\phi = \sigma, \omega^0, \rho^0$ and A^0 , which are determined by the Klein-Gordon equation in cylindrical coordinates. Thus a set of coupled equations, namely the Dirac equation with potential terms for the nucleons and the Klein-Gordon type equations with sources for the mesons and the photon is obtained. These equations are solved self consistently. For this purpose, as described above, the well-tested basis expansion method has been employed [32, 54]. For further details of these formulations we refer the reader to refs. [32, 48, 54].

3. Results and Discussion

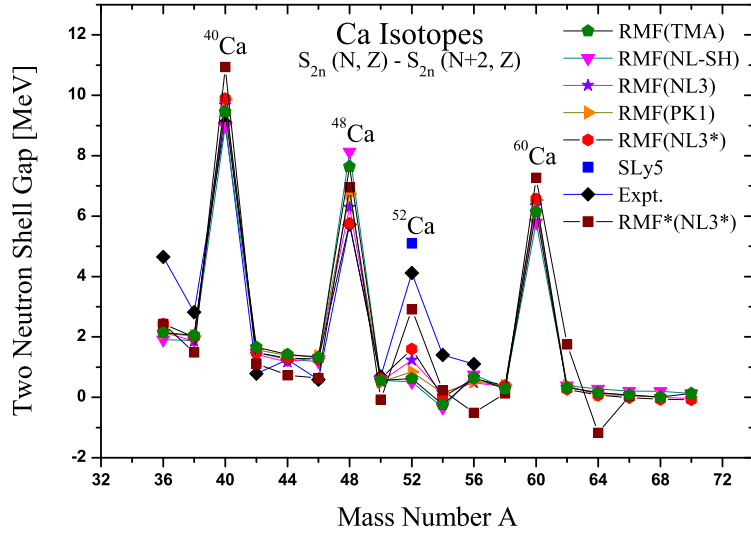


Figure 1: (Colour online) Two neutron shell gap [$S_{2n}(N, Z) - S_{2n}(N+2, Z)$] for Ca Isotopes calculated through various parameters. For comparison experimental data [72] and the data calculated by tensor interaction (SLy5) [18] are also shown. RMF* is representing RMF calculations done using mass dependent pairing.

Magic numbers between $N(Z) = 20$ to $N(Z) = 50$ are mainly governed by position and separation of single particle states in and from pf shell. For a detailed study in this region towards neutron and proton side, we first carry out RMF+BCS calculations including the deformation degree of freedom (referred to throughout as deformed RMF) to search spherical or nearly spherical isotones/isotopes. It is found that some isotones/isotopes actually exhibit very small or almost no deformation. Therefore, for such cases of negligible deformation, we take advantage to use RMF+BCS approach for spherical shapes (referred to throughout as RMF) for the analysis of results. This description in terms of spherical single particle wave functions and energy levels treats shell closures and magicity etc. with more convenience and transparency. Addition to this, with the spherical framework of RMF pairing gaps, total pairing energy, contributions of neutron and proton single particle states etc. can be demonstrated with more clarity.

To study pf shell, we first turn on our discussion with emergence of new shell closures ($N = 32$ and 34) in exotic Ca isotopes which have been indicated by recent experiments [12, 13, 14, 15]. First it was observed that due to high excitation energy of ^{52}Ca as compared to its neighbouring nuclei, $N = 32$ shell closure may develop [73, 74]. After that from recent high-precision mass measurements of several isotopes ranging from ^{51}Ca up to ^{54}Ca a confirmation was obtained in 2013 [13]. In addition, from the more recent measurement of the 2_1+ energy in ^{54}Ca , it is also found that ^{54}Ca could be magic as well [14].

To investigate the possibility for ^{52}Ca and ^{54}Ca , we have displayed two neutron shell gap [$S_{2n}(N, Z) - S_{2n}(N+2, Z)$] in Fig. 1 which is determined by calculations of RMF with different sets of parameters i.e. TMA [49], NLSH [50], NL3 [51], PK1 [52] and NL3* [53]. Ca isotopes have been examined with TMA and NL-SH parameters in Ref [40] in detail where constant pairing strength $V_0 = 350 \text{ MeV fm}^3$ has been used. This constant pairing strength $V_0 = 350 \text{ MeV fm}^3$ has been also used in the description of other magic nuclei [46, 47]. We have used the same pairing strength for other parameters also and the results are shown together with available experimental data [72] and the available data of calculations recently done by Skyrme parameter set with tensor interaction (SLy5) [18] for comparison.

It is reflected from the Fig. 1 that calculations done in Ref [40] with TMA & NLSH parameter and the calculations with other parameters retrace well with the experimental data throughout for all isotopes of Ca, however for ^{52}Ca and ^{54}Ca these results are not reproducing experimental peaks in a

good agreement. As can be seen from Fig. 1, for Ca isotopes the results of TMA & NLSH parameters [40] along with NL3 & PK1 parameter are far enough with the experimental results. However, NL3* is showing better results but even these results for ^{52}Ca and ^{54}Ca are not in a good agreement with experimental data. As mentioned above, we apply mass dependent pairing also for our calculations and we use NL3* parameter which is found with better agreement comparative to other parameters. It is indeed gratifying to note that mass dependent pairing together with NL3* parameter considerably improves result of ^{52}Ca as can be seen from Fig. 1. These results for complete chain of Ca isotopes are mentioned with RMF* in the diagram shown by magenta square.

Obtaining better peak in Fig. 1 for ^{52}Ca with RMF*(NL3*), one can also observed sudden peaks for known other doubly magic nuclei viz. ^{40}Ca and ^{48}Ca . In addition to this, from Fig. 1, no indication is found for magic character of ^{54}Ca . Moving further, there is again a large peak for ^{60}Ca much stronger than ^{52}Ca and similar to the peaks obtained in ^{40}Ca and for ^{48}Ca giving indication of more strong doubly magic nucleus ^{60}Ca . With the recent experiments on Ca isotopes [13, 14] next doubly magic nucleus ^{60}Ca is predicted here for future experiments which may be an interesting and remarkable finding due to its doubly magicity and its position near neutron drip-line of Ca. The above results for $^{52,54,60}\text{Ca}$ are further supported by pairing energy contribution from protons and neutrons, separation energies and wavefunction characteristics.

From the above discussion it would be important to investigate neutron shell closures $N = 32, 34$ and 40 in detail for full isotonic chains upto their driplines. In addition from the isospin symmetry considerations [11], it would be also useful to study proton shell closures $Z = 32, 34$ and 40 for full isotopic chains upto their driplines. Therefore, in the following we will examine these isotonic/isotopic chain in detail using RMF approach with mass dependent pairing using NL3* parameter which has produced better outcome over constant pairing strength and various other parameters as shown above in the case of ^{52}Ca .

3.1. $N = 32$ and 34

It is very interesting example and situation for various theoretical and experimental studies to study $N = 32$ and $N = 34$ shell closure simultaneously, therefore in the following discussion we will examine $N = 32$ and $N = 34$ within the framework of RMF theory using nuclei ^{52}Ca and ^{54}Ca .

To show the magicity of $N = 32$ or $N = 34$, we choose some spherical or nearly spherical nuclei in the isotopic chain of Si, Ca and Ni. It has been shown through various studies [20, 75, 76] and we have also found using deformed RMF approach [47, 48] that expect a few cases all the nuclei in Ca and Ni isotopic chain are spherical or nearly spherical in nature. Conversely, many of the Si isotopes are found strongly deformed through various experimental and theoretical studies [8, 10]. However, $^{22,34,48}\text{Si}$ are found to have spherical shapes which has been shown already using deformed RMF approach [46]. From deformed RMF approach it is found that ^{42}Si exhibits shape coexistence with an oblate ground state being the deformation parameter $\beta_2 = -0.37$ [46, 77]. Moving towards neutron rich side for $^{44,46,48}\text{Si}$ the second minimum becomes less pronounced gradually and for drip-line isotope ^{48}Si only one minima contributes indicating completely spherical ground state configuration. This comment, allow us to choose $^{46,48}\text{Si}$ as nearly spherical/spherical nuclei for our study. In the following discussion we mainly select ^{46}Si , ^{52}Ca and ^{60}Ni to investigate shell closure at $N = 32$, and ^{48}Si , ^{54}Ca and ^{62}Ni for shell closure at $N = 34$ using spherical RMF approach.

With these above remarks, in Fig. 2, we display our results of neutron single particle energies for isotonic chain of $N = 28, 30, 32$ and 34 . These results are obtained using NL3* parameter [53] with considering mass dependency on pairing strength. We have also mentioned experimental values of single particle energies of known doubly magic nucleus [22, 78]. These values are marked with filled star in left lower panel and it is grateful to note that our calculated single particle energies using NL3* parameter and mass dependent pairing are indeed very close to the experimental values specially for ^{48}Ca which earmark us to be interpretative for the study of shell closures on the basis of single particle energy.

The gap after neutron $1f_{7/2}$ state is well reflected from the figure in ^{48}Ca and ^{56}Ni as shown in lower left panel of Fig. 2. However this shell gap gets weakened in ^{42}Si suggesting a disappearance of $N = 28$ shell closure similar to refs. [6, 8, 9, 10]. This weakening can be caused and inferred by inclusion of deformations which is a matter of separate discussion in the main context of this paper. Now moving towards more neutron rich case for $N = 32$ (right upper panel), the next 4 neutrons ($28 + 4 = 32$ Neutrons) are filled in the states $2p_{3/2}$ and $2p_{1/2}$ located above the $1f_{7/2}$ state. From right upper panel in Fig. 2, it is evident that $2p_{3/2}$ and $2p_{1/2}$ states are very close to each other in ^{46}Si , and are occupied by these four neutrons simultaneously. However, moving towards higher Z (from $Z = 14$ to $Z = 20$)

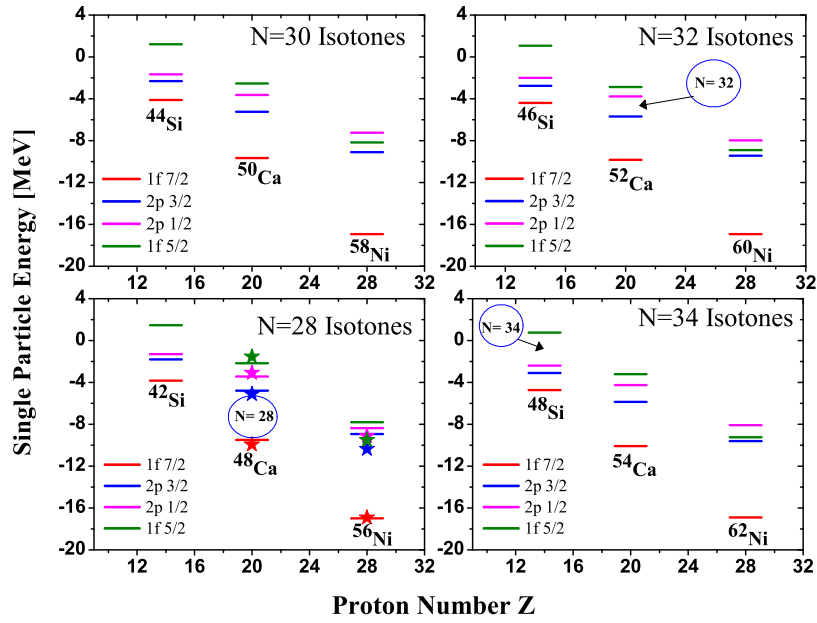


Figure 2: (Colour online) Variation of neutron single particle states for Si, Ca and Ni isotopes constituting neutron number $N = 28, 30, 32$ and 34 in all four panel respectively. These results are calculated using mass dependent pairing with NL3* parameter. Left lower panel is also showing available experimental single particle energies of doubly magic nuclei [22, 78].

i.e. in ^{52}Ca , these two states $2p_{3/2}$ and $2p_{1/2}$ get separated as shown in the Fig. 2 for $N = 32$ isotones. This separation results a shell gap at $N = 32$ in ^{52}Ca which is similar to recent results [12, 13]. It is also observed from the Fig. 2 that the state having higher angular momentum (neutron $1f_{5/2}$) moves deeper on increasing proton number (Si to Ni). For Si isotopes, $1f_{5/2}$ state is far separated from closely situated $2p_{3/2}$ and $2p_{1/2}$ states. Whereas for Ca isotopes due to more protons this $1f_{5/2}$ state is quite close to $2p_{1/2}$ state resulting a gap after $2p_{3/2}$ state which may even lead to $N = 32$ shell closure. However, this shell gap is not so strong as it has been found for any conventional magic number such as gap after $1f_{7/2}$ in ^{48}Ca as shown in left lower panel. Moving towards more proton rich side in Ni isotopes, this state $1f_{5/2}$ moves even below to $2p_{3/2}$ and $2p_{1/2}$ states and therefore this filling in of $1f_{5/2}$ state before $2p_{3/2}$ and $2p_{1/2}$ states declines the possibility of $N = 32$ shell gap in ^{60}Ni or in further proton rich nuclei.

From the Fig. 2, it is also apparent that for $N = 34$ isotones (right lower panel) for lower Z the state $1f_{5/2}$ lies significantly above from the states $2p_{3/2}$ and $2p_{1/2}$ as shown in the case of ^{48}Si and gives rise to new shell closure at $N = 34$ for lower Z nuclei like Si. It can also be anticipated that due to large gap as reflected from Fig. 2, $N = 34$ shell closure behaves more strongly than that of $N = 32$ shell closure. Consequently, ^{48}Si may be considered as a more strong spherical doubly magic candidate for the future experiments in the same mass region as that of ^{52}Ca .

To check the dependency of parameters on the above results of $N = 32$ and $N = 34$ shell closures, it would be important and interesting to go through the calculations with different sets of parameters. With this in view, in the Table 1, we have tabulated results using few more parameters for comparison. We have performed the RMF calculations with mass dependent pairing strength using TMA [49], NLSH [50], NL3 [51], PK1 [52] and NL3* [53] force parameters. The energy gaps between $2p_{3/2}$ and $2p_{1/2}$ states for $N = 32$ and between $2p_{1/2}$ and $1f_{5/2}$ states for $N = 34$ are tabulated for different parameters sets in Table 1.

From Table 1, it is clear that for ^{52}Ca , the similar shell gap between $2p_{3/2}$ and $2p_{1/2}$ states also lies for other parameters. Using mass dependent pairing with TMA & NLSH parameter (see column 3 and 4) this gap is rather small [1.48 MeV for TMA and 1.59 MeV for NLSH] comparative to other parameters (column 5, 6, 7), but it is found larger than the gap calculated using constant pairing strength in Ref [40]. With the calculations in Ref [40], this gap is found 1.37 MeV and 1.48 MeV with TMA and NL-SH parameter

Table 1: Shell gap responsible for magicity of ^{52}Ca and ^{48}Si are shown using various parameters

Nucleus	Gap between states	Shell Gap [MeV]				
		RMF* (Mass Dependent Pairing)				
		TMA	NLSH	NL3	PK1	NL3*
^{52}Ca	$2p_{3/2}$ and $2p_{1/2}$	1.48	1.59	1.85	1.58	1.90
^{48}Si	$2p_{1/2}$ and $1f_{5/2}$	2.89	2.90	3.11	3.00	3.15

respectively. Therefore from here it may be concluded with the comparison that calculation considered here with mass dependent pairing provides a better treatment over constant pairing calculation as done in Ref [40] specially for new shell closure in Ca isotopes. In a similar manner, the gap between $2p_{1/2}$ and $1f_{5/2}$ states is found significant by other parameters resulting a more strong shell closure at $N = 34$ for ^{48}Si . It is important to note here from the Table 1 that present results with NL3* parameter are more supportive and certificatory for other sets of parameters.

To get further support for above results of shell closure at ^{52}Ca we have displayed in Fig. 3, occupancy (number of neutrons) of neutron single particle states $1f_{7/2}$, $2p_{3/2}$, $2p_{1/2}$ and $1f_{5/2}$ (pf shell) for the nuclei ^{46}Si , ^{52}Ca , ^{60}Ni from $N = 32$ isotonic chain using TMA, NL-SH, NL3, PK1 and NL3* parameters. Very first observation from Fig. 3 is that our results from all parameters are similar. It can be also observed that for all parameters, occupancy of state $1f_{7/2}$ is unchanged for all considered nuclei. However, occupancy for other neutron states $2p_{3/2}$, $2p_{1/2}$ and $1f_{5/2}$ change significantly. From the Fig. 3, it is evident that occupancy of $1f_{5/2}$ state for ^{46}Si is zero as $1f_{5/2}$ lies around 3 MeV above than $2p_{3/2}$ and $2p_{1/2}$ states as mentioned in Table 1. In ^{46}Si these two states $2p_{3/2}$ and $2p_{1/2}$ are occupied together but moving towards ^{52}Ca , occupancy of $2p_{1/2}$ state decreases and becomes zero. This is rather very essential for development of $N = 32$ shell closure along with $2p_{3/2}$ should attain its maximum occupancy. Occupancy of $2p_{1/2}$ becomes exactly zero and occupancy of $2p_{3/2}$ state increases upto its maximum and it accommodates all four neutrons with $2p_{1/2}$ and $1f_{5/2}$ vacant. The gap therefore between $2p_{3/2}$ and $2p_{1/2}$ leads to shell closure characteristic at $N = 32$. As said above, all the parameters are favourable and clearly showing magicity at $N = 32$ as can be seen from Fig. 3. Moving further towards ^{60}Ni state $1f_{5/2}$ goes much deeper due to which it accommodates more particles

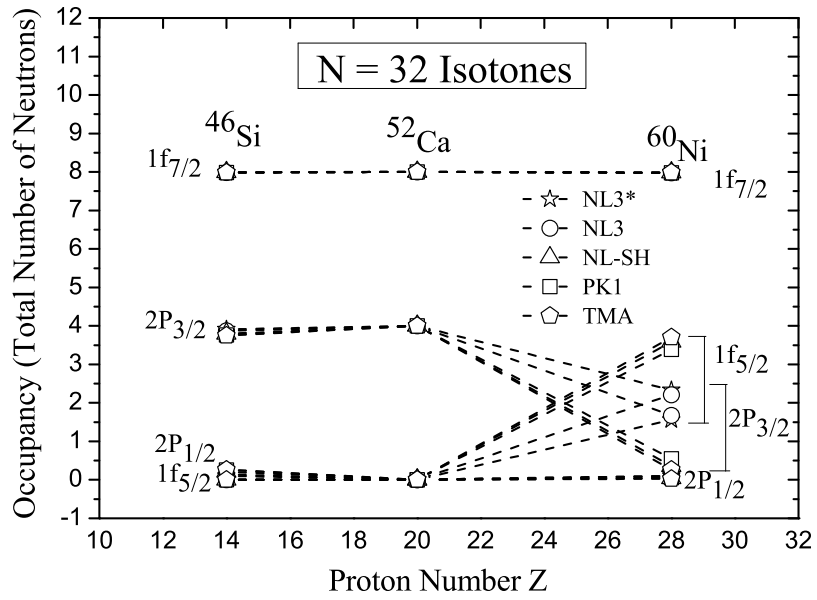


Figure 3: Variation of occupancy (no. of neutrons) for various neutron single particle states for N = 32 isotones (⁴⁶Si, ⁵²Ca and ⁶⁰Ni).

than $2p_{3/2}$ and hence destroys the shell closure which has developed for ^{52}Ca . The calculations from TMA, NL-SH, NL3, PK1 and NL3* provide same sort of results and behaviour of these states.

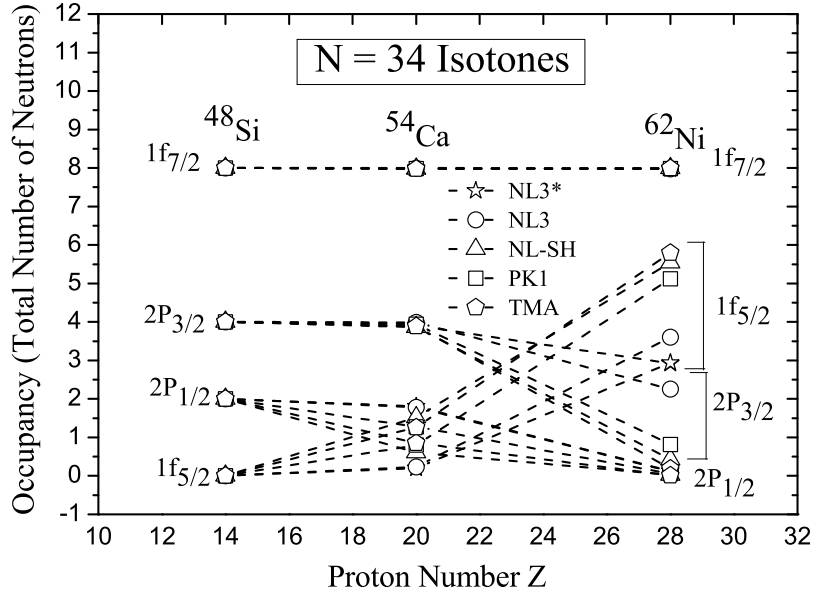


Figure 4: Same as Fig. 3 but for $N = 34$ isotones (^{48}Si , ^{54}Ca and ^{62}Ni).

Next in Fig. 4, we have shown occupancy (number of neutrons) of neutron single particle pf states for the nuclei ^{48}Si , ^{54}Ca , ^{62}Ni from $N = 34$ isotonic chains. From Fig. 4, it can be observed that $2p_{3/2}$ and $2p_{1/2}$ states are fully occupied for ^{48}Si and $1f_{5/2}$ is having zero occupancy. This result is same for all parameters and hence supporting magic character of $N = 34$ in ^{48}Si . It is worth here to point out that moving from ^{48}Si to ^{54}Ca occupancy of $2p_{3/2}$ and $2p_{1/2}$ states decreases whereas occupancy of $1f_{5/2}$ state increases upto ^{62}Ni . Because of this filling in of $1f_{5/2}$ state together with $2p_{3/2}$ and $2p_{1/2}$ states in ^{54}Ca there is no possibility of $N = 34$ shell closure in ^{54}Ca or in higher nuclei. However, this kind of uniform filling of $1f_{5/2}$ state is not observed in ^{52}Ca as illustrated above and in Fig. 3. Therefore, it can be concluded here that ^{52}Ca and ^{48}Si are found to possess magic character and there are no sign

found for shell closure at $N = 34$ in ^{54}Ca .

3.2. $Z = 32$ and 34

After the discussion on neutron shell closure at $N = 32$ and 34 , it is expected from the isospin symmetry considerations [11] that towards proton side $Z = 32$ and $Z = 34$ should also exhibit similar shell closures. With this in view, in a similar manner, we have performed our deformed RMF+BCS calculations for isotopic chain of $Z = 32$ and $Z = 34$. Most of the nuclei in the isotopic chains are found deformed but it is also found that there are several nuclei which are actually spherical or nearly spherical. These are $^{60,82,114}\text{Ge}$ for $Z = 32$ and $^{62,84,116}\text{Se}$ for $Z = 34$ corresponding to $N = 28, 50$ and 82 . It is important to note that these nuclei cover complete isotopic chain from proton rich side to neutron rich side as one moves from $N = 28$ to $N = 82$. It is worth to mention here that $N = 82$ is found to be neutron drip-line for Ge ($Z=32$) and Se ($Z=34$) isotopic chains.

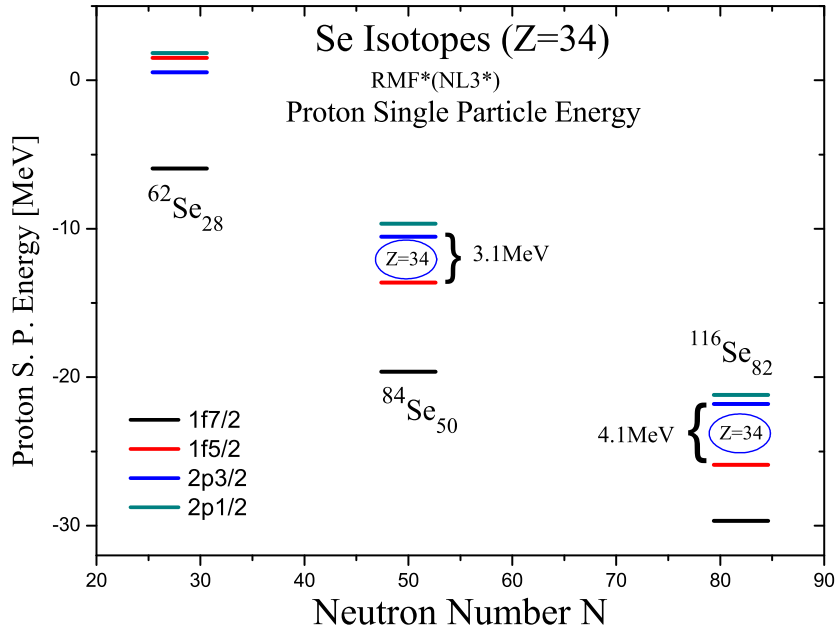


Figure 5: (Colour Online) Proton single particle energies of $1f_{7/2}$, $1f_{5/2}$, $2p_{3/2}$ and $2p_{1/2}$ states for Se ($Z=34$) isotopes.

For these nuclei, we have performed spherical RMF+BCS calculations using mass dependent pairing with NL3* parameter and it is gratifying to note that $Z = 34$ indeed shows shell closure characteristic towards neutron rich side. To elaborate this, in Fig. 5, we display our results of proton single particle energy for all above mentioned nuclei. From Fig. 5, it is observed that proton $1f_{5/2}$ state lies in between $2p_{3/2}$ and $2p_{1/2}$ states initially for proton rich side at ^{62}Se . Moving towards neutron rich side $1f_{5/2}$ state goes down to these $2p_{3/2}$ and $2p_{1/2}$ states, consequently, creates a significant gap (3.1 MeV for $N = 50$ and 4.1 MeV for $N = 82$) and gives rise to strong shell closure at $Z = 34$ for the nuclei with $N = 50$ and $N = 82$. Therefore, our calculations predict $^{84,116}\text{Se}$ as doubly magic nuclei giving rise to shell closure at $Z = 34$ similar to $N = 34$. Moreover, pairing energy contribution from proton and neutron is also found zero which supports the magic character of both these nuclei $^{84,116}\text{Se}$.

Comparatively, it can be concluded that towards neutron side ($N = 32$) empty $1f_{5/2}$ state lies above on $2p_{3/2}$ and $2p_{1/2}$ for ^{52}Ca gives rise to $N = 32$ shell closure but toward proton side for $Z = 32$ isotopes $1f_{5/2}$ state always lies below to $2p_{3/2}$ and $2p_{1/2}$ states and thus proton filling in $1f_{5/2}$ state just after $1f_{7/2}$ state ($28+6 = 34$) gives no probability of $Z = 32$ shell closure. It should be also mentioned here that ^{116}Se and ^{48}Si both are drip-line nuclei for $Z = 34$ and $Z = 14$ respectively and these new shell closures at $Z = 34$ and $N = 34$ are due to reorganization of single particle levels in the vicinity of drip-lines. Again, these results have been tested for different box radius and consistency is found in the above said conclusions.

3.3. $N = 40$ and $Z = 40$

The gap created by pf shell with $1g_{9/2}$ state is responsible for the shell closure at $N = 40$ or $Z = 40$. Therefore it would be again interesting to investigate behaviour of pf shell, consequently respective positions of single particle states of pf shell and $1g_{9/2}$ state for $N(Z) = 40$. To visualize this shell closure we have performed calculations for all isotones of $N = 40$ and isotopes of $Z = 40$ with deformed RMF+BCS approach as done in the previous subsections and found that $N = 40$ is spherical for neutron rich side ranging from $Z = 16$ to $Z = 30$ having zero quadrupole deformation parameter ($\beta_2 = 0$), whereas $Z = 40$ (Zr) is spherical for only $N = 50$ and $N = 82$. For these nuclei once again we have applied spherical RMF+BCS approach using mass dependent pairing with NL3* parameter and some of the results are plotted in Fig. 6.

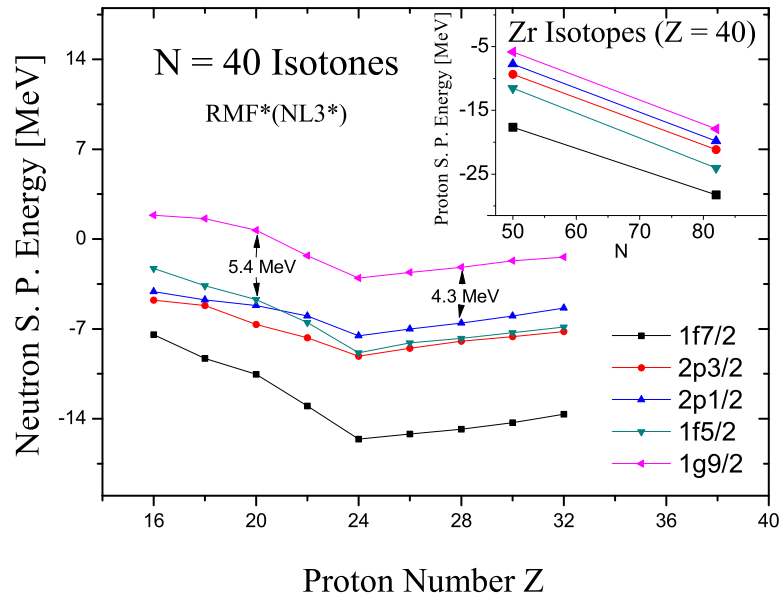


Figure 6: (Colour online) Variation of neutron single particle energy of pf shell and $1g_{9/2}$ state with respect to proton number Z for N = 40 isotones. The inset shows proton single particle energies for same states but for Z = 40 isotopes as a function of Neutron number N.

We have shown proton single particle energy of various states for $N = 40$ isotones with $Z = 16 - 32$. From the Fig. 6, it is evident that $N = 40$ shell closure is due to gap between neutron pf shell and neutron $1g_{9/2}$ state. But the variation in the positions of states of pf shell, this gap changes as one moves from $Z = 16$ to $Z = 32$. For $Z = 16 - 20$ neutron $1f_{5/2}$ state lies above to the $2p_{3/2}$ and $2p_{1/2}$ and variation is such that gap between $1g_{9/2}$ and $1f_{5/2}$ states increases from $Z = 16$ to $Z = 20$. At $Z = 20$ for ^{60}Ca $1f_{5/2}$ produces the gap with $1g_{9/2}$ at its maximum value 5.4 MeV as can be seen from Fig. 6. Moving towards higher Z ($Z > 20$), $1f_{5/2}$ state gets deeper because of its higher angular momentum as compared to $2p_{3/2}$ and $2p_{1/2}$ states. Moving beyond $Z = 20$, this gap responsible for $N = 40$ now arises between $2p_{1/2}$ and $1g_{9/2}$, and for $Z = 28$ it is found 4.3 MeV which results ^{68}Ni as a candidate of doubly magicity. This doubly magic candidate ^{68}Ni has been identified by Broda et al. [79] and recently by Bentley et al. [80].

We have also analyzed the behaviour of pf shell in $Z = 40$ (Zr) isotopes. In a similar manner we found only two isotopes which are spherical i.e. ^{90}Zr and ^{122}Zr as mentioned above. For these isotopes, it is seen that there is no reorganization of proton pf shell ($1f_{7/2}$, $1f_{5/2}$, $2p_{3/2}$ and $2p_{1/2}$ states) and proton $1g_{9/2}$ state. These states follow the same positions while moving from ^{90}Zr to ^{122}Zr as can be seen in the inset of Fig. 6. It is found that the energy gap between pf shell and $1g_{9/2}$ state for ^{90}Zr and ^{122}Zr is around 1 MeV which is not so pronounced. Therefore for Zr isotopes, $Z = 40$ is not found to be a proton shell closure dissimilar to above discussed $N = 40$ neutron shell closure.

Important outcome of the above study is the appearance of $N = 40$ shell closure for $Z = 16$ to $Z = 30$. Among these nuclei, ^{60}Ca and ^{68}Ni are much pronounced shell closures as mentioned above (gap is 5.4 MeV and 4.3 MeV respectively as mentioned also in Fig. 6). As already stated that recently magicity of the nucleus ^{52}Ca is confirmed by employing the mass spectrometer of ISOLTRAP at CERN [13]. So far mass of ^{58}Ca is known [72, 81] and therefore one may expect the determination of mass in ^{60}Ca in near future.

3.4. Ground state properties of predicted magic nuclei in pf shell

With the above detailed investigations, we predict shell closure at ^{52}Ca and strong shell closures at ^{60}Ca , ^{48}Si , ^{68}Ni along with $^{84,116}\text{Se}$ in pf shell. For all of these nuclei the calculations are carried out within the framework of deformed RMF approach (axially deformed configuration) and these calculations have yielded valuable results related to the ground state properties,

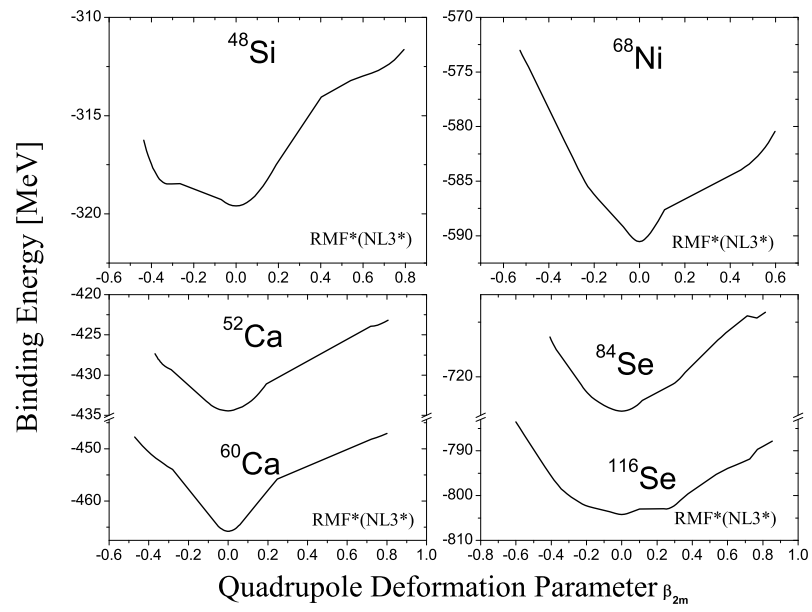


Figure 7: The potential energy surface of $^{52,60}\text{Ca}$, ^{48}Si , ^{68}Ni and $^{84,116}\text{Se}$ as a function of the deformation parameter β_2 .

Table 2: Ground state properties of ^{52}Ca , ^{60}Ca , ^{48}Si , ^{68}Ni , ^{84}Se and ^{116}Se

Properties	^{52}Ca	^{60}Ca	^{48}Si	^{68}Ni	^{84}Se	^{116}Se
B. E. (MeV)	434.452	465.752	319.590	590.525	726.236	804.216
S_{2p} (MeV)	34.893	45.842	52.259	27.695	25.750	47.927
S_{2n} (MeV)	9.90	7.049	2.445	15.770	15.374	0.767
R_c (fm)	3.512	3.639	3.262	3.859	4.114	4.475
R_p (fm)	3.419	3.550	3.163	3.776	4.036	4.403
R_n (fm)	3.832	4.153	4.046	4.040	4.282	5.133
R_m (fm)	3.681	3.962	3.810	3.933	4.184	4.930
β_2	0.00	0.00	0.00	0.00	0.00	0.00
Pairing Energy (MeV)	0.00	0.00	0.00	0.00	0.00	0.00

such as binding energy, rms proton and neutron radii, two proton and two neutron separation energies, deformations etc. It will be interesting to get more insight into the shapes of these nuclei. In Fig. 7, we have plotted binding energy curves as function of quadrupole deformation parameter as obtained with constrained RMF calculations including the deformation degree of freedom for all above nuclei. From Fig. 7, it is valuable to note that all these nuclei show a spherical ground state configuration which validate all the above results interpreted by using spherical RMF approach. A sharp minima is readily seen in ^{60}Ca comparable to ^{52}Ca suggesting a more strong spherical character in ^{60}Ca . Similarly very sharp minima are also observed for ^{68}Ni , ^{84}Se and ^{116}Se . In Table 2, we present here some important ground state properties of these nuclei calculated by axially deformed RMF approach using NL3* parameter.

Moreover, guided from the predicted shell closures and for systematic comparison with experimental data we have also calculated ground state properties of chains of isotopes of Si, Ca, Ni and Se isotopes using axially deformed RMF approach with NL3* parameter. In Fig. 8, we have plotted two neutron separation energy S_{2n} for chains of isotopes of Si, Ca, Ni and Se nuclei. To demonstrate the validity of RMF calculations, we have also compared our results of two neutron separation energy with one of the popular nonrelativistic approach viz. Skyrme-Hartree-Fock method with the HFB-17 functional given by Goriely et al. [82]. From Fig. 8 it is evident that results of RMF calculations are in fairly good agreement with available experimental data and the results of Skyrme-Hartree-Fock method for all three chains of isotopes. For Si isotopes, the two neutron separation energy becomes neg-

ative after $N = 34$ with RMF calculations and concludes that two neutron drip line for Si isotopes is $N = 34$. Interestingly this nucleus of Si with $N = 34$ (^{48}Si) is one of our predicted doubly magic nucleus as mentioned earlier and leads to an example of drip line doubly magic nucleus with new neutron magic number $N = 34$. However, with HFB calculations [82] this nucleus ^{48}Si is little unbound with 0.46 MeV resulting two neutron drip line at $N = 32$ for Si isotopes. In a similar way drip lines for Ca, Ni and Se isotopes with RMF calculations are found at $N = 46$, $N = 70$ and at $N = 82$ respectively. Therefore, our predicted doubly magic nucleus ^{60}Ca is near to drip line of Ca and once again another predicted doubly magic nucleus ^{116}Se represents an interesting example of drip line doubly magic nucleus with new proton magic number $Z = 34$. From HFB calculations the drip lines are found at little variance $N = 48$, $N = 64$ and $N = 80$ for Ca, Ni and Se isotopes respectively. A sharp decrease in the value of S_{2n} just after magic number can be seen from the Fig. 8. This sharp fall lies after ^{48}Si , ^{52}Ca , ^{60}Ca , ^{68}Ni , ^{84}Se and ^{116}Se affirming our conclusions. Other properties of these isotopic chains and similar systematic calculations for chains of isotones of $N = 32$, 34 and 40 (not shown here) are found with excellent agreement with available experimental data [72] along with HFB calculations [82] and over again fortify our predictions.

4. Summary

In the present investigation we have employed the relativistic mean-field plus BCS (RMF+BCS) approach [47, 48] to study shell closures $N(Z) = 32$, 34 and 40 in neutron and proton pf shell extensively. For our study, the RMF calculations for all the nuclei considered here have been firstly carried out assuming a deformed shape (deformed RMF) and then the situation where nuclei are ascertained exhibiting very small or almost no deformation has been beneficially utilized by employing spherical RMF approach. For our calculation, mass dependent pairing is found more suitable and effective over constant pairing to cover a large mass region. The main body of the results of our calculations includes single particle spectra, two proton and two neutron separation energies and other ground state properties for complete isotonic and isotopic chain. For the description we have applied mainly NL3* [53] parameter and used various other popular force parameters viz. TMA [49], NL-SH [50], NL3 [51] and PK1 [52] to testify our results and outcomes.

One of the prime reason of this study is to investigate neutron and proton

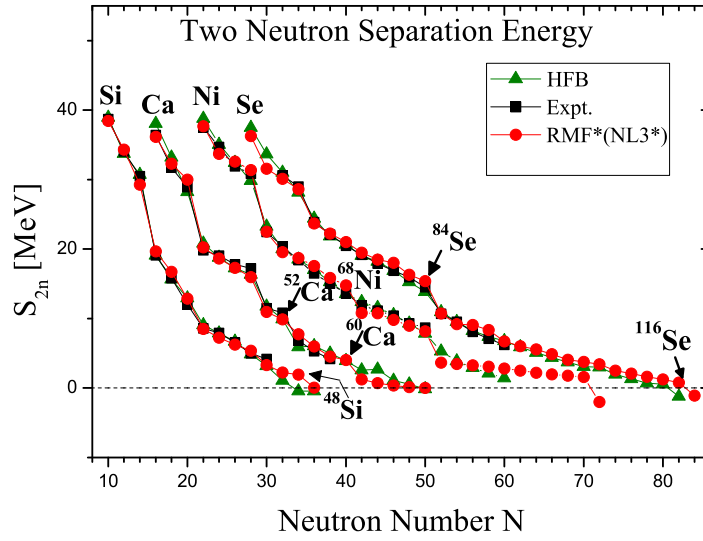


Figure 8: (Colour online) The two neutron separation energy for Si, Ca, Ni and Se isotopes are obtained with axially deformed RMF approach and compared with the Skyrme-Hartree-Fock calculations [82]. Figure also depicts the available experimental data [72] for the purpose of comparison.

single particle states of pf shell and consequently appearance of new shell closures. The main force behind this study is recent experimental observation showing new magicity at $N = 32$ and 34 [12, 13, 14, 15]. We have found through single particle energies and separation energies that $N = 32$ behaves like a shell closure in ^{52}Ca which is in accord of recent observation, whereas $N = 34$ is not showing shell closure in ^{54}Ca . But, $N = 34$ is found to possess more strong shell closure in proton deficient nucleus ^{48}Si which is an example of doubly magic drip-line nucleus and potential candidate for future experiments in the same mass region as that of ^{52}Ca . Towards proton side $Z = 32$ is not found to exhibit magic character but $Z = 34$ becomes closed and resulting doubly magic nuclei $^{84,116}\text{Se}$ out of which ^{116}Se is again an example of doubly magic drip-line nucleus. In addition to this, we have also focused on shell closure $N(Z) = 40$ and came up that $N = 40$ shows shell closure towards proton deficient side resulting doubly magicity in ^{60}Ca and ^{68}Ni . Out of these nuclei the gap between neutron pf shell and next neutron $1g_{9/2}$ state responsible of $N = 40$ shell closure, is maximum for ^{60}Ca . Our further study of two neutron shell gap for Ca isotopes also confirms that ^{60}Ca is possibly another important doubly magic nucleus near drip-line next to ^{52}Ca for future experiments.

Acknowledgements

Authors would like to thank Prof. H. L. Yadav, Banaras Hindu University, Varanasi, INDIA for his kind guidance and continuous support. The authors are indebted to Prof. L. S. Geng, Beihang University, China for valuable correspondence. One of the authors (G. Saxena) gratefully acknowledges the support provided by Science and Engineering Research Board (DST), Govt. of India under the young scientist project YSS/2015/000952.

References

- [1] A. Ozawa, T. Kobayashi, T. Suzuki, K. Yoshida, and I. Tanihata, Phys. Rev. Lett. 84 (2000) 5493.
- [2] R. Kanungo et al., Phys. Rev. Lett. 102 (2009) 152501.
- [3] C. R. Hoffman et al., Phys. Lett. B 672 (2009) 17.
- [4] K. Tshoo, et al., Phys. Rev. Lett. 109 (2012) 022501.

- [5] H. Iwasaki et al., Phys. Lett. B 481 (2000) 7.
- [6] B. Bastin et al., Phys. Rev. Lett. 99 (2007) 022503.
- [7] S. Watanabe et al., Phys. Rev. C 89 (2014) 044610.
- [8] B. Jurado et al., Phys. Lett. B 649 (2007) 43.
- [9] D. Tarpanov, H. Liang, N. Van Giai and C. Stoyanov, Phys. Rev. C 77 (2008) 054316.
- [10] S. Takeuchi et al., Phys. Rev. Lett. 109 (2012) 182501.
- [11] T. Otsuka and A. Schwenk, Nucl. Phys. News 22(4) (2012) 12.
- [12] A. Gade, et al., Phys. Rev. C 74 (2006) 021302(R).
- [13] F. Wienholtz, et al., Nature 498 (2013) 346.
- [14] D. Steppenbeck, et al., Nature 502 (2013) 207.
- [15] M. Rosenbusch et al., Phys. Rev. Lett. 114 (2015) 202501.
- [16] A. T. Gallant et al., Phys. Rev. Lett. 109 (2012) 032506.
- [17] J. J. Li, J. Margueron, W. H. Long and N. Van Giai, Physics Letters B, 753 (2016) 97.
- [18] M. Grasso, Phys. Rev. C 89 (2014) 034316.
- [19] Z. H. Wang, J. Xiang, W. H. Long and Z. P. Li, Journal of Phys. G. 42 (2015) 045108.
- [20] J. Meng et al., Phys. Rev. C 65 (2002) 041302(R).
- [21] D. Vautherin and M. Veneroni, Phys. Lett. B 29 (1969) 203.
- [22] D. Vautherin and D. M. Brink, Phys. Rev. C 5 (1972) 626.
- [23] J. Dechargé and D. Gogny, Phys. Rev. C 21 (1980) 1568.
- [24] B. D. Serot and J. D. Walecka, Adv. Nucl. Phys. 16 (1986) 1.
- [25] J. Boguta, A. R. Bodmer, Nucl. Phys. A 292 (1977) 413.

- [26] J. Terasaki, P. H. Heenen, H. Flocard and P. Bonche, Nucl. Phys. A 600 (1996) 371.
- [27] K. Bennaceur, J. Dobaczewski and M. Ploszajczak, Phys. Lett. B 496 (2000) 154.
- [28] M. Grasso, N. Sandulescu, Nguyen Van Giai and R. J. Liotta, Phys. Rev. C 64 (2001) 064321.
- [29] N. Sandulescu, Nguyen Van Giai and R. J. Liotta, Phys. Rev. C 61 (2000) 061301(R).
- [30] A. Bouyssy, J.-F. Mathiot, Nguyen Van Giai, and S. Marcos, Phys. Rev. C 36 (1987) 380.
- [31] P-G Reinhard, Rep. Prog. Phys. 52 (1989) 439.
- [32] P. Ring, Y. K. Gambhir and G. A. Lalazissis, Comput. Phys. Commun. 105 (1997) 77 and reference therein.
- [33] Y. Sugahara and H. Toki, Nucl. Phys. A 579 (1994) 557.
- [34] P. Ring, Prog. Part. Nucl. Phys. 37 (1996) 193.
- [35] M. M. Sharma, M. A. Nagarajan and P. Ring, Phys. Lett. B 312 (1993) 377.
- [36] J. Meng, Nucl. Phys. 635 (1998) 3.
- [37] G. A. Lalazissis, D. Vretenar and P. Ring, Phys. Rev. C 57 (1998) 2294.
- [38] S. Mizutori, J. Dobaczewski, G. A. Lalazissis, W. Nazarewicz and P. G. Reinhard, Phys. Rev. C 61 (2000) 044326.
- [39] M. Del Estal, M. Contelles, X. Vinas and S. K. Patra, Phys. Rev. C 63 (2001) 044321.
- [40] H. L. Yadav, M. Kaushik and H. Toki, Int. Jour. Modern Physics E 13 (2004) 647.
- [41] H. L. Yadav, S. Sugimoto and H. Toki, Mod. Phys. Lett. A 17 (2002) 2523.

- [42] J. Meng, H. Toki, J.Y. Zeng, S. Q. Zhang and S. Q. Zhou, Phys. Rev. C 65 (2002) 041302(R).
- [43] Y. Utsuno et al., Phys. Rev. C 86 (2012) 051301(R).
- [44] M. Grasso and M. Anguiano, Phys. Rev. C 92 (2015) 054316.
- [45] H. Sagawa and G. Colo, Progress in Particle and Nuclear Physics 76 (2014) 1.
- [46] G. Saxena, D. Singh, M. Kaushik, and S. Somorendro Singh, Canadian Journal of Physics 92 (2014) 253.
- [47] G. Saxena, D. Singh, M. Kaushik, H. L. Yadav and H. Toki, Int. Jour. Mod. Phys. E 22 (2013) 1350025.
- [48] D. Singh, G. Saxena, M. Kaushik, H. L. Yadav and H. Toki, Int. Jour. Mod. Phys. E 21 (2012) 1250076.
- [49] L. S. Geng, H. Toki, A. Ozawa and J. Meng, Nucl. Phys. A 730 (2004) 80.
- [50] G. A. Lalazissis, D. Vretenar and P. Ring, Phys. Rev. C 63 (2001) 034305.
- [51] G.A. Lalazissis, Physical Review C 55 (1997) 540.
- [52] W. Long, J. Meng, N. Van Giai and Shan-Gui Zhou, Physical Review C 69 (2004) 034319.
- [53] G. A. Lalazissis, S. Karatzikos, R. Fossion, D. Pena Arteaga, A. V. Afanasjev, and P. Ring, Phys. Lett. B 671 (2009) 36.
- [54] L. S. Geng, H. Toki, S. Sugimoto and J. Meng, Prog. Theor. Phys. 110 (2003) 921.
- [55] T. Niksic, D. Vretenar, P. Finelli, and P. Ring, Phys. Rev. C 66 (2002) 024306.
- [56] G. A. Lalazissis, T. Niksic, D. Vretenar, and P. Ring, Phys. Rev. C 71 (2005) 024312.

- [57] X. Roca-Maza, X. Vinas, M. Centelles, P. Ring, and P. Schuck, Phys. Rev. C 84 (2011) 54309.
- [58] P. Ring, Journal of Physics: Conference Series 49 (2006) 93.
- [59] K. Heyde and J. L. Wood, Rev. Mod. Phys. 83 (2011) 1467.
- [60] T. Otsuka and Y. Tsunoda, J. Phys. G: Nucl. Part. Phys. 43 (2016) 024009.
- [61] L. S. Ferreira, E. Maglione and P. Ring, EPJ Web of Conf. 117 (2016) 06004.
- [62] Xing Hu Li et al., Int. J. Mod. Phys. D 25 (2016) 1650002.
- [63] S. Mehta, H. Kaur, B. Kumar, and S. K. Patra Phys. Rev. C 92 (2015) 054305.
- [64] J. Sugano, H. Kouno, M. Yahiro, Phys. Rev. D 94 (2016) 014024.
- [65] W. Nazarewicz, T.R. Werner, and J. Dobaczewski, Phys. Rev. C 50 (1994) 2860.
- [66] J. Dobaczewski, W. Nazarewicz, T. R. Werner, J. F. Berger, C. R. Chinn, and J. Decharge, Phys. Rev. C 53 (1996) 2809.
- [67] N. Sandulescu, L.S. Geng, H. Toki and G. Hillhouse, Phys. Rev. C 68 (2003) 054323.
- [68] Lane A. M., "Nuclear Theory", Benjamin, (1964).
- [69] Ring P. and Schuck P., "The Nuclear many-body Problem", Springer (1980).
- [70] J. Dobaczewski, H. Flocard and J. Treiner, Nucl. Phys. A 422 (1984) 103.
- [71] G. F. Bertsch and H. Esbensen, Ann. Phys. (N.Y.), 209 (1991) 327.
- [72] G. Audi et al., Chinese Physics C 36 (2012) 1287.
<http://www.nndc.bnl.gov/>
- [73] J. I. Prisciandaro et al., Phys. Lett. B 510 (2001) 17.

- [74] D. C. Dinca et al., Phys. Rev. C 71 (2005) 041302.
- [75] W. Ning and L. Min, Chinese Science Bulletin 60 (2015) 1145.
- [76] H. Grawe and M. Lewitowicz , Nucl. Phys. A 693 (2001) 116.
- [77] G.A. Lalazissis, D. Vretenar, P. Ring, M. Stoitsov, and L.M. Robledo, Phys. Rev. C 60 (1999) 014310.
- [78] L. Trache et al. Phys. Rev., C 54 (1996) 2361.
- [79] R. Broda et al., Phys. Rev. Lett. 74 (1995) 868.
- [80] I. Bentley, Y. Coln Rodriguez, S. Cunningham, and A. Aprahamian, Phys. Rev. C 93 (2016) 044337.
- [81] M. Wang et al., Chin. Pys. C 36 (2012) 1603.
- [82] S. Goriely et al., Phys. Rev. Lett. 102 (2009) 152503, <http://www-astro.ulb.ac.be/bruslib/>.